

## Molecular Basis for the Electric Field Modulation of Cytochrome *c* Structure and Function

Pablo M. De Biase,<sup>†</sup> Damián Alvarez Paggi,<sup>†</sup> Fabio Doctorovich,<sup>†</sup>  
Peter Hildebrandt,<sup>‡</sup> Dario A. Estrin,<sup>†</sup> Daniel H. Murgida,<sup>\*,†</sup> and Marcelo A. Marti<sup>\*,†,§</sup>

*Departamento de Química Inorgánica, Analítica, y Química Física, Facultad de Ciencias Exactas y Naturales, Universidad de Buenos Aires, INQUIMAE-CONICET, Ciudad Universitaria, Pab. 2, C1428EHA, Buenos Aires, Argentina, Institut für Chemie, Technische Universität Berlin, Str. des 17. Juni 135, Sekr. PC14, D10623 Berlin, Germany, and Departamento de Química Biológica, Facultad de Ciencias Exactas y Naturales, Universidad de Buenos Aires. Ciudad Universitaria, Pab. 2, C1428EHA, Buenos Aires, Argentina*

Received August 8, 2009; E-mail: dhmurgida@qi.fcen.uba.ar; marcelo@qi.fcen.uba.ar

**Abstract:** Cytochrome *c* (Cyt) is a small soluble heme protein with a hexacoordinated heme and functions as an electron shuttle in the mitochondria and in early events of apoptosis when released to the cytoplasm. Using molecular dynamics simulations, we show here that biologically relevant electric fields induce an increased mobility and structural distortion of key protein segments that leads to the detachment of the sixth axial ligand Met80 from the heme iron. This electric-field-induced conformational transition is energetically and entropically driven and leads to a pentacoordinated high spin heme that is characterized by a drastically lowered reduction potential as well as by an increased peroxidase activity. The simulations provide a detailed atomistic picture of the structural effects of the electric field on the structure of Cyt, which allows a sound interpretation of recent experimental results. The observed conformational change may modulate the electron transfer reactions of Cyt in the mitochondria and, furthermore, may constitute a switch from the redox function in the respiratory chain to the peroxidase function in the early events of apoptosis.

### 1. Introduction

Mechanisms of biological energy transduction and conversion, as well as many enzymatic processes, rely upon charge transfer reactions as key steps.<sup>1</sup> Examples are light-driven water splitting in photosynthesis and oxidative phosphorylation in respiratory chains, where the energy provided by a downhill cascade of electron transfer (ET) events is utilized for proton translocation across a membrane. In both cases the electrochemical gradient sustained by this proton-coupled ET activity is utilized for driving ATP synthesis. The machinery consists of protein complexes that are an integral part of the membrane, while smaller molecules that can diffuse within the membrane or in the membrane–solution interface act as electron shuttles. This is the case for cytochrome *c* (Cyt), a soluble monohemic protein that transports electrons from complex III to the terminal enzyme cytochrome *c* oxidase (CcO) in the mitochondrial respiratory chain. A very unique aspect of this type of system is that the integral and peripherally bound redox proteins involved must stand relatively high local electric fields (EFs). Such fields arise from different ion concentrations at both sides of the membrane, the distribution of charged and uncharged lipid head groups, and the alignment of molecular dipoles of lipids and water

molecules in the membrane–solvent interfaces. As a result, EF strengths at interfaces may approach values of up to 100 mV Å<sup>-1</sup>,<sup>2</sup> which are likely to affect structures and processes of integrated and membrane-attached proteins. Although the action of electrical potentials has been identified as determinant for several biological processes, including nerve excitation, transport, and energy transduction,<sup>3–14</sup> only for a few cases are the underlying EF-induced structural changes of the proteins involved well understood. In the specific case of respiratory

<sup>†</sup> Departamento de Química Inorgánica, Analítica, y Química Física, Universidad de Buenos Aires.

<sup>‡</sup> Technische Universität Berlin.

<sup>§</sup> Departamento de Química Biológica, Universidad de Buenos Aires.

(1) Wikström, M. *Biophysical and Structural Aspects of Bioenergetics*; RSC Publishing: Cambridge, 2005.

- (2) Clarke, R. J. *Adv. Colloid Interface Sci.* **2001**, *89*, 263–281.  
 (3) Franzen, S.; Goldstein, R. F.; Boxer, S. G. *J. Phys. Chem.* **1990**, *94* (12), 5135–5149.  
 (4) Geibel, S.; Friedrich, T.; Ormos, P.; Wood, P. G.; Nagel, G.; Bamberg, E. *Biophys. J.* **2001**, *81* (4), 2059–2068.  
 (5) Gopher, A.; Blatt, Y.; Schönfeld, M.; Okamura, M. Y.; Feher, G.; Montal, M. *Biophys. J.* **1985**, *48* (2), 311–320.  
 (6) Markin, V. S.; Liu, D.; Gimsa, J.; Strobel, R.; Rosenberg, M. D.; Tsong, T. Y. *J. Membr. Biol.* **1992**, *126* (2), 137–145.  
 (7) Nachmansohn, D.; Neumann, E. *Chemical and Molecular Basis of Nerve Activity*; Academic Press: New York, 1975.  
 (8) Nagel, G.; Kelety, B.; Möckel, B.; Büldt, G.; Bamberg, E. *Biophys. J.* **1998**, *74* (1), 403–412.  
 (9) Ren, D.; Navarro, B.; Xu, H.; Yue, L.; Shi, Q.; Clapham, D. E. *Science* **2001**, *294* (5550), 2372–2375.  
 (10) Slatin, S. L.; Nardi, A.; Jakes, K. S.; Baty, D.; Duché, D. *Proc. Natl. Acad. Sci. U.S.A.* **2002**, *99* (3), 1286–1291.  
 (11) Tsong, T. Y. *J. Biol. Phys.* **2002**, *28* (2), 309–325.  
 (12) Abriata, L. A.; Cassina, A.; Tortora, V.; Marin, M.; Souza, J. M.; Castro, L.; Vila, A. J.; Radi, R. *J. Biol. Chem.* **2009**, *284* (1), 17–26.  
 (13) Song, Y. Y.; Li, Y.; Yang, C.; Xia, X. H. *Anal. Bioanal. Chem.* **2008**, *390* (1), 333–341.  
 (14) Song, Y. Y.; Jia, W. Z.; Yang, C.; Xia, X. H. *Adv. Funct. Mater.* **2007**, *17* (14), 2377–2384.

chains the possible effect of EFs is largely unexplored, although it has been noticed in early studies that relatively large transmembrane potentials may cause a substantial decrease of the enzymatic activity of CcO toward Cyt.<sup>15–17</sup>

It is well established that the electrostatic interaction of the positively charged Cyt with negatively charged model systems, such as phospholipid vesicles,<sup>18,19</sup> polyelectrolytes,<sup>20</sup> or the binding domain of the natural reaction partner CcO,<sup>21</sup> may promote the formation of the conformation state B2, in which the axial Met80 ligand is removed from the heme iron. At physiological pH, this coordination site may remain vacant (five-coordinated high spin, 5cHS) or may be occupied by a histidine residue.<sup>22,23</sup> The disruption of the Fe–Met80 bond alters the properties of Cyt in a significant way. On the one hand, the B2 state has a reduction potential that is more than 300 mV lower than that of the native protein (state B1).<sup>24,25</sup> On the other hand, the B2 state shows a substantial increase of its peroxidase activity by allowing the access of hydrogen peroxide to the heme iron.<sup>26,27</sup> Thus, *in vivo* the B1 → B2 transition would have profound physiological consequences since the B2 state cannot accept electrons from complex III but is capable of catalyzing the peroxidation of cardiolipin,<sup>27</sup> the major charged lipid component of the inner mitochondrial membrane.<sup>28</sup> The degradation of cardiolipin has been suggested to increase the permeability of the membrane, thus facilitating the transfer for Cyt to the cytosol where it binds to Apaf-1, one of the initial events in apoptosis.<sup>26,27</sup> Thus, it appears to be likely that the switch from the “normal” redox function of Cyt (B1 state) to the apoptotic function (B2 state) depends on the local electric field, which in turn is modulated by the membrane potential.

In previous work, using surface-enhanced resonance Raman spectroscopy, we have investigated the structure of Cyt electrostatically bound to electrodes coated with anionic films.<sup>24</sup>

Variation of the electrode potential and the charge density on the film surface shows that the equilibrium between the B1 and B2 states of the protein is shifted toward B2 upon raising the EF strength at the interface of the biomimetic devices. It has also been shown that the orientation of Cyt in electrostatic complexes can be controlled through the EF strength<sup>13,14,29,30</sup> and that high fields are associated to a gain of peroxidase electrocatalytic activity, probably due to the formation of the B2 state.<sup>13,14</sup>

On the basis of these observations, we investigated the influence of the EF on the dissociation energy of the Fe–Met80 bond in model porphyrins using density functional theory (DFT).<sup>31</sup> In that case, i.e., for the isolated heme complex lacking the protein environment, no significant effect on the Fe–S bond stability was predicted for biologically meaningful EF strengths.

Here we present a molecular dynamics (MD) simulations study of Cyt, in the presence of moderate EFs. The results show that moderate EFs induce an increased mobility and structural distortion of protein segments that result in the formation of the state B2.

## 2. Computational Methods

**2.1. System Setup.** The initial structure of Cyt was obtained from the PDB entry 1HRC<sup>32</sup> and corresponds to the crystallographic structure of the ferric protein. Missing hydrogens were added to the PDB structure using the *tleap* module of the Amber package.<sup>33,34</sup> For ionizable residues we assigned the standard protonation state at physiological pH, leading to a protein net charge of +8. To set up the system for molecular dynamics (MD) simulations the starting structure was immersed into a 10 Å truncated octahedral box of TIP3P water molecules, including eight chloride counterions. The final system contained the protein, 5102 water molecules, and 8 chloride anions leading to a total of 17,059 atoms. Three additional bonds between the protein chain residues and the heme were introduced: one between the proximal His18NE and the heme iron, (N–Fe), and one in each of the vinyl groups of the heme with the sulfur atoms of Cys14 and Cys17 (C–S), to simulate the c-type heme. Finally, for simulations of the native protein (state B1) an additional bond between the Met80 sulfur and the heme iron was introduced (Fe–Met80).

**2.2. MD Simulation Parameters.** All simulations were performed at 300 K and 1 bar, maintained with the Berendsen barostat and thermostat,<sup>35</sup> using periodic boundary conditions and Ewald sums (grid spacing of 1 Å) for treating long-range electrostatic interactions.<sup>36,37</sup> The SHAKE algorithm<sup>38</sup> was used to keep bonds involving hydrogen atoms at their equilibrium length. A 2 fs time

- (15) Gregory, L.; Ferguson-Miller, S. *Biochemistry* **1989**, *28* (6), 2655–2662.
- (16) Nicholls, P.; Butko, P. J. *Bioenerg. Biomembr.* **1993**, *25* (2), 137–143.
- (17) Sarti, P.; Antonini, G.; Malatesta, F.; Brunori, M. *Biochem. J.* **1992**, *284* (1), 123–127.
- (18) Bernad, S.; Oellerich, S.; Soulimane, T.; Noinville, S.; Baron, M. H.; Paternostre, M.; Lecomte, S. *Biophys. J.* **2004**, *86* (6), 3863–3872.
- (19) Droghetti, E.; Oellerich, S.; Hildebrandt, P.; Smulevich, G. *Biophys. J.* **2006**, *91* (8), 3022–3031.
- (20) Weidinger, I. M.; Murgida, D. H.; Dong, W. F.; Möhwald, H.; Hildebrandt, P. *J. Phys. Chem. B* **2006**, *110* (1), 522–529.
- (21) Döpner, S.; Hildebrandt, P.; Rosell, F. I.; Mauk, A. G.; von Walter, M.; Buse, G.; Soulimane, T. *Eur. J. Biochem.* **1999**, *261* (2), 379–391.
- (22) Oellerich, S.; Wackerbarth, H.; Hildebrandt, P. *J. Phys. Chem. B* **2002**, *106* (25), 6566–6580.
- (23) Note that the coordination of the heme iron in the conformational state B2, which is formed at neutral pH, differs with respect to the so-called states IV and V formed under alkaline conditions.<sup>22</sup>
- (24) Murgida, D. H.; Hildebrandt, P. *Acc. Chem. Res.* **2004**, *37* (11), 854–861.
- (25) The conformational state B1 refers to the electrostatically bound protein, which is spectroscopically and electrochemically indistinguishable from the native protein in solution, i.e., from the so-called state III.
- (26) Godoy, L. C.; Muñoz-Pinedo, C.; Castro, L.; Cardaci, S.; Schonhoffa, C. M.; King, M.; Tórtora, V.; Marín, M.; Miao, Q.; Jiang, J. F.; Kapralov, A.; Jemmerson, R.; Silkstone, G. G.; Patel, J. N.; Evans, J. E.; Wilson, M. T.; Green, D. R.; Kagan, V. E.; Radi, R.; Mannick, J. B. *Proc. Natl. Acad. Sci. U.S.A.* **2009**, *106* (8), 2653–2658.
- (27) Kagan, V. E.; Tyurin, V. A.; Jiang, J.; Tyurina, Y. Y.; Ritov, V. B.; Amoscato, A. A.; Osipov, A. N.; Belikova, N. A.; Kapralov, A. A.; Kini, V.; Vlasova, I. I.; Zhao, Q.; Zou, M.; Di, P.; Svistunenko, D. A.; Kurnikov, I. V.; Borisenko, G. G. *Nat. Chem. Biol.* **2005**, *1* (4), 223–232.
- (28) Róg, T.; Hector, M. S.; Munck, N.; Oresic, M.; Karttunen, M.; Vattulainen, I. *J. Phys. Chem. B* **2009**, *113* (11), 3413–3422.

- (29) Kranich, A.; Ly, H. K.; Hildebrandt, P.; Murgida, D. H. *J. Am. Chem. Soc.* **2008**, *130* (30), 9844–9848.
- (30) Alvarez Paggi, D.; Martín, D. F.; Kranich, A.; Hildebrandt, P.; Martí, M. A.; Murgida, D. H. *Electrochim. Acta* **2009**, *54* (22), 4963–4970.
- (31) De Biase, P. M.; Doctorovich, F.; Murgida, D. H.; Estrin, D. A. *Chem. Phys. Lett.* **2007**, *434* (1–3), 121–126.
- (32) Bushnell, G. W.; Louie, G. V.; Brayer, G. D. *J. Mol. Biol.* **1990**, *214*, 585.
- (33) Case, D. A.; Darden, T. A.; Cheatham, T. E.; Simmerling, C. L.; Wang, J.; Duke, R. E.; Luo, R.; Crowley, M.; Walker, R. C.; Zhang, W.; Merz, K. M.; Wang, B.; Hayik, S.; Roitberg, A.; Seabra, G.; Kolossváry, I.; Wong, K. F.; Paesani, F.; Vanicek, J.; Wu, X.; Brozell, S. R.; Steinbrecher, T.; Gohlke, H.; Yang, L.; Tan, C.; Mongan, J.; Hornak, V.; Cui, G.; Mathews, D. H.; Seetin, M. G.; Sagui, C.; Babin, V.; Kollman, P. A. *AMBER 10*; University of California: San Francisco, 2008.
- (34) Pearlman, D. A.; Case, D. A.; Caldwell, J. W.; Ross, W. S.; Cheatham III, T. E.; DeBolt, S.; Ferguson, D.; Seibel, G.; Kollman, P. *Comput. Phys. Commun.* **1995**, *91* (1–3), 1–41.
- (35) Berendsen, H. J. C.; Postma, J. P. M.; Van Gunsteren, W. F.; DiNola, A.; Haak, J. R. *J. Chem. Phys.* **1984**, *81*, 3684–3690.
- (36) Darden, T.; York, D.; Pedersen, L. J. *J. Chem. Phys.* **1993**, *98*, 10089–10092.

step for the integration of Newton's equations was used. The nonbonded cutoff radii were 12 Å. The AMBER99 force field<sup>39</sup> parameters were used for all residues, except for the heme. The heme parameters were developed and thoroughly tested by our group in previous works.<sup>40,41</sup> All simulations were performed with the PMEMD module of the AMBER9 package.<sup>33,34</sup> Some modifications have been introduced to the PMEMD module to allow simulation of a uniform electric field and a Morse potential bond as described below.

An equilibration protocol was applied that consists in performing an energy minimization by optimizing the initial structure, followed by a slow heating to the desired temperature using a linear temperature ramp from 100 to 300 K during 80 ps at constant volume and a subsequent pressure stabilization run at 300 K and 1 bar during 100 ps. Position frames, which were used for analyzing trajectories, were collected at 2 ps intervals. Production MD simulations consisted of four 50 ns simulations: (i) without applied EF and with the structure constrained to the B1 state by the introduction of the Fe-Met80 bond (B1); (ii) without applied EF and without the Fe-Met80 bond (B2); (iii) B1 state with an applied EF (B1EF); and (iv) B2 state with an applied EF (B2EF).

**2.3. Application of a Homogeneous Electric Field.** The force vector  $\vec{F}$  generated by the application of a uniform external electric field  $\vec{E}_F$  on the  $i^{\text{th}}$  atom with partial charge  $q$  was calculated as

$$\vec{F}_i = q_i \vec{E}_F \quad (1)$$

The energy  $U$  associated with the interaction of the applied field with all of the atoms of the system is calculated as

$$U = - \sum_{i=1}^n q_i \vec{r}_i \cdot \vec{E}_F = - \vec{d} \cdot \vec{E}_F \quad (2)$$

where  $\vec{r}$  is the position vector of atom  $I$ ,  $\vec{d}$  is the electric dipolar moment, and  $n$  is the total number of atoms. Unless stated otherwise, all calculations were performed with an applied electric field strength of 25 mV Å<sup>-1</sup>, which is about one-fourth of the strength estimated for a fully saturated phosphatidylcoline membrane model.<sup>2</sup> The field vector was chosen to be parallel to the total dipole of the initial protein structure.

**2.4. Free Energy Profiles of the Fe-Met80 Bond Dissociation with and without Electric Field.** To obtain thermodynamic information of the Fe-Met80 dissociation process, free energy profiles were computed. The profiles were constructed by performing constant velocity multiple steered molecular dynamics (MSMD) simulations and using Jarzynski's equality,<sup>42</sup> which relates equilibrium free energy ( $\Delta G$ ) values with the irreversible work performed over the system, which proceeds along a reaction coordinate from reactants to products, according to

$$e^{\frac{\Delta G(\xi)}{k_B T}} = \left\langle e^{\frac{W(\xi)}{k_B T}} \right\rangle \quad (3)$$

where  $W(\xi)$  is the external work performed on the system as it evolves from the initial to the final state along the reaction coordinate ( $\xi$ ), computed by integrating the force acting on the steering potential along  $\xi$ . The steering potential  $E(\xi)$  is a harmonic well that moves with constant velocity ( $v$ ) along the reaction coordinate, so

$$E(\xi) = k[\xi - (\xi_0 + v\Delta t)]^2 \quad (4)$$

The reaction coordinate was chosen as the Fe(heme)–S(Met80) distance. Calculations were performed using a force constant of 400 kcal mol<sup>-1</sup> Å<sup>-2</sup> and a pushing velocity of 3 Å ns<sup>-1</sup>, with and without applied electric field. A set of 20 MSMD simulations were performed in the association direction. The starting structures for each MSMD simulations were taken randomly from the frames of the previous MD runs. Two different free energy profiles were constructed, with and without applied electric field (25 mV Å<sup>-1</sup>). Since the coordination transition involves the formation/breaking of a bond, a process that is not allowed in the standard MD force field, we introduced a Morse potential to describe the bond potential ( $V$ ):

$$V = D(1 - e^{-a(r-r_e)})^2 \quad (5)$$

The parameters used here correspond to the equilibrium distance  $r_e$  (2.362 Å), the dissociation energy constant  $D$  (13.84 kcal mol<sup>-1</sup>), and the width parameter of the potential  $a$  (1.77 Å<sup>-1</sup>), which is related to the force constant of the bond ( $k$ ) by

$$a = \sqrt{\frac{k}{2D}} \quad (6)$$

This parametrization was performed using DFT based QM calculations with the SIESTA code<sup>43,44</sup> as described previously,<sup>31</sup> using Fe<sup>III</sup>-porphyrin, dimethylthiol, and 5-methylimidazole as models for the heme, methionine, and histidine, respectively. The ground spin state of all species was determined by calculating the energies of the low, intermediate, and high spin states. The  $D$  parameter was determined as the dissociation energy of the dimethylthiol from the iron, and the  $a$  parameter was determined by fitting the Morse potential to the energy of structures obtained by moving the S–Fe distance near the equilibrium distance.

**2.5. Origin-Independent Electric Dipole Moment.** The origin-independent electric dipole moment  $\vec{p}$  is computed for a set of  $n$  atoms with partial charges  $q_i$  and positions  $\rightarrow r_i$  as:

$$\vec{p} = \sum_{i=1}^n (q_i - q_0) \vec{r}_i = \vec{d} - Q \vec{r}_0 \quad (7)$$

where  $q_0 = 1/n \sum_i q_i$ ,  $\vec{d} = \sum_i q_i \vec{r}_i$ ,  $Q = nq_0$ , and  $\vec{r}_0 = 1/n \sum_i r_i$ .  $\vec{d}$  is the dipole moment defined as usual for neutral systems,  $Q$  is the total charge of the protein, and  $\vec{r}_0$  is the position vector of the geometric center of the  $n$  of atoms. Subtraction of  $q_0$ , the monopole component, makes the result independent of the choice of the origin whatever the charge of the system is.

**2.6. Origin-Independent Electric Field Energy ( $\Delta E_{\text{EF}}$ ).** The expression to calculate the energy of the protein under the influence of the applied uniform electric field is described in eq 2. As the protein is a charged particle, the energy depends on the position of the protein with respect to the origin. To have an electric field energy independent of the origin position, we define  $\Delta E_{\text{EF}}$  as

$$\Delta E_{\text{EF}} = U + Q \vec{r}_0 \cdot \vec{E}_F = - \vec{p} \cdot \vec{E}_F \quad (8)$$

where all parameters are the same as defined in eqs 2 and 7.  $\Delta E_{\text{EF}}$  is the electric field energy minus the electrostatic energy component given by the monopole under the constant electric field.

(37) Essmann, U.; Perera, L.; Berkowitz, M. L.; Darden, T.; Lee, H.; Pedersen, L. G. *J. Chem. Phys.* **1995**, *103*, 8577–8593.

(38) Ryckaert, J. P.; Ciccolini, G.; Berendsen, H. J. C. *J. Comput. Phys.* **1977**, *23*, 327–341.

(39) Cheatham, T. E.; Cieplak, P.; Kollman, P. A. *J. Biomol. Struct. Dyn.* **1999**, *16* (4), 845–862.

(40) Nádra, A. D.; Marti, M. A.; Pesce, A.; Bolognesi, M.; Estrin, D. A. *Proteins* **2008**, *71* (2), 695–705.

(41) Perissinotti, L. L.; Marti, M. A.; Doctorovich, F.; Luque, F. J.; Estrin, D. A. *Biochemistry* **2008**, *47* (37), 9793–9802.

(42) Jarzynski, C. *Phys. Rev. Lett.* **1997**, *78* (14), 2690–2693.

(43) Reich, S.; Thomsen, C.; Ordejon, P. *Phys. Rev. B* **2002**, *65* (15), 155411.

(44) Soler, J. M.; Artacho, E.; Gale, J. D.; Garcia, A.; Junquera, J.; Ordejon, P.; Sanchez-Portal, D. *J. Phys.: Condens. Matter* **2002**, *14* (11), 2745–2779.

**2.7. Calculation of Thermodynamic Parameters.** Thermodynamic parameters were calculated using the MM-PBSA approach as implemented in the AMBER9 package. It combines the molecular mechanical energies with a continuum solvent approach. Molecular mechanical energies are determined with the *SANDER* program and represent the internal energy terms (bond, angle, and dihedral) and van der Waals and electrostatic interactions energies terms. An infinite cutoff for all interactions is used. The electrostatic contribution to the solvation free energy is calculated with a numerical solver for the Poisson–Boltzmann (PB) method or by generalized Born (GB) methods implemented in *SANDER*.<sup>33,34</sup>

Conformational entropy calculations were performed by diagonalization of the mass weighted Cartesian covariance matrix, using the Schlitter<sup>45</sup> and the Andricioaei-Karplus<sup>46</sup> methods. Since the sampling in a MD simulation depends on the length of the simulation, the calculated entropy also depends on the length of the trajectory used for the calculation. To obtain a value that does not depend on the trajectory length, we calculated the entropy for increasing intervals of 2.4 ns and fitted the entropy values to the following expression:

$$S(t) = S_{\infty} - \frac{\alpha}{(t - t_0)^{2/3}} \quad (9)$$

where  $S_{\infty}$  corresponds to the entropy when time approaches infinity, and  $\alpha$  and  $t_0$  are independent parameters. This procedure has been previously described by Harris et al.<sup>47</sup> For the calculations, we considered the backbone atoms of residues 3 to 102.

### 3. Results

**3.1. Structure and Dynamics of the Native Cytochrome *c*.** The structural dynamics of native Cyt (state B1) was analyzed by performing 50 ns long MD simulations using the crystallographic structure of the ferric protein as starting point. As shown in Figure 1, the root-mean-square distance (RMSd) of the backbone atoms remains largely constant along the simulation with deviations of ca. 2.2 Å with respect to the reference crystallographic structure. Maxima deviations are observed at 24 and 45 ns, where the RMSd values rise to about 2.4 Å due to slight movements of the less ordered loops. The RMSd between the crystal structure and the B1 average structure of the 50 ns simulation is 2.04 Å in the absence of an external electric field (see Table 1).

In the presence of a homogeneous electric field of 25 mV Å<sup>-1</sup> applied parallel to the dipole moment, Cyt exhibits a distorted and more flexible structure (B1EF), with an oscillating RMSd that can reach values close to 3.5 Å and an average value of 2.35 Å (Figure 1, Table 1).

Computation of the RMSd values for the B1 and B1EF using the average structures of the last 46 ns of the simulations as a reference show that both ensembles are stable (Supporting Information, Figure S11 and Table 1).

The structural fluctuations of the native protein are largely restricted to certain segments, as observed upon computation of the root-mean-square fluctuations (RMSf) for the individual residues, which are indicative of the mobility of the protein structure (Figure 2, lower panel). On the basis of this analysis, contiguous secondary structure elements can be grouped into greater segments and classified as flexible (F) or rigid (R) as

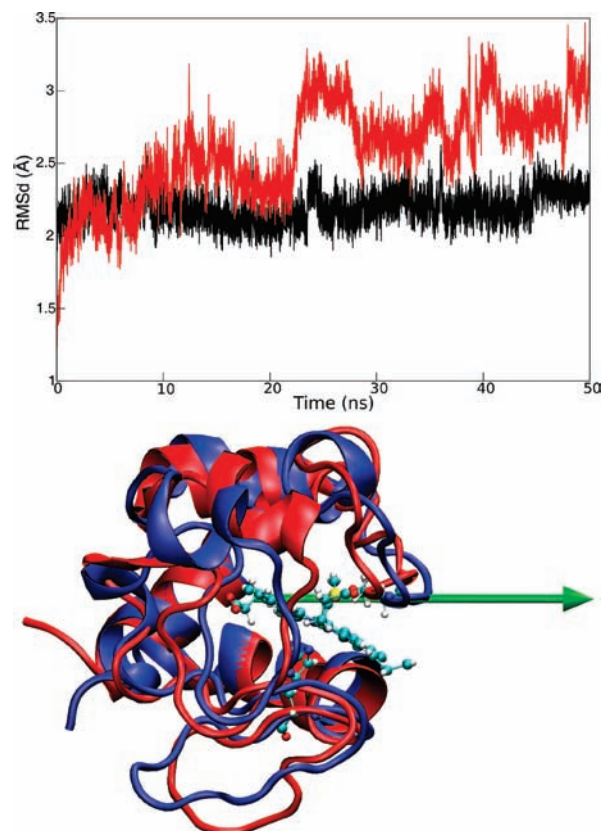


**Figure 1.** Upper panel: time evolution of the RMSd of the backbone atoms for B1 (black line) and B1EF (red line) with respect to the X-ray crystal structure. Lower panel: B1 (blue) versus B1EF (red) average structures and B1 dipolar moment vector (green arrow).

**Table 1.** Average RMSd Calculated with Respect to Starting X-ray Crystal Structure from 4th to 50th ns of the Dynamic and RMSd between Crystal Structure and Average Structure

states	av RMSd for starting X-ray crystal structures (Å)	RMSd between crystal and average structures (Å)
B1	2.197 ± 0.105	2.037
B1EF	2.643 ± 0.292	2.354
B2*	2.222 ± 0.248	1.830
B2EF*	3.593 ± 0.322	3.190

shown in Table 2. Note that both the N- and C-terminus helices (H1 and H4, respectively) are included in rigid segments. In general terms, the rigid segments include the more stable secondary structure elements, such as long helices (more than 7 residues) and long hydrogen-bonded turns (more than 5 residues). In contrast, the flexible segments are comprised by loops (coils), short helices, short sheets, and turns.

Upon application of a homogeneous electric field the RMSd value increases for all Cyt residues, but significant changes are observed only for the flexible segments. This mobility increase is accompanied by structural changes of the protein, which becomes evident in Figure 2 (upper panel), where the  $\alpha$ -carbon distance between the B1 and B1EF average structures is plotted as a function of the residue number.

Note that the crucial residue for the B1 → B2 structural transition, Met80, is included in one of the flexible segment (F4). The EF-induced motion of this particular residue appears overdamped by the fact that these MD simulations do not contemplate a possible break down of the Fe–Met80 bond.

(45) Schlitter, J. *Chem. Phys. Lett.* **1993**, *215* (6), 617–621.

(46) Andricioaei, I.; Karplus, M. *J. Chem. Phys.* **2001**, *115* (14), 6289–6292.

(47) Harris, S. A.; Gavathiotis, E.; Searle, M. S.; Orozco, M.; Laughton, C. A. *J. Am. Chem. Soc.* **2001**, *123* (50), 12658–12663.

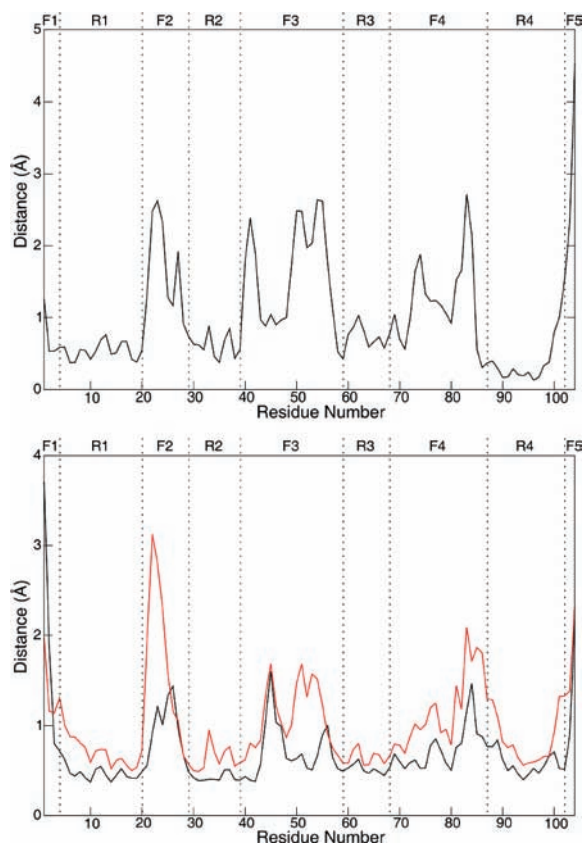


**Figure 2.** Upper panel:  $C_{\alpha}$  distance versus residue plot between B1 and B1EF average structures. Lower panel: root mean square fluctuations (RMSF) versus residue for both the B1 (black line) and B1EF (red line) states.

However, the magnitude of the structural changes observed for the F4 segment suggests that electric fields of moderate intensity might be able to induce the transition.

**3.2. Structure and Dynamics of the Five-Coordinated Cytochrome *c*.** To assess the structural flexibility of the five-coordinated Cyt, 50 ns long MD simulations were performed starting from the crystallographic structure of ferric Cyt and removing the Fe–Met80 bond from the force field. Thus, the structure may be considered as a “precursor” for the formation of state B2 since the stable B2 state differs from the native B1 state by major alterations of the tertiary structure.<sup>18,22</sup> We will, therefore, refer to this structural model as the B2\* state. As shown in Figure 3, the RMSd of the B2\* state with respect to the crystal structure evolves in time with amplitude variations larger than the native state B1, although the B2\* state average structure deviates only 1.83 Å from the crystal, i.e., very similar to B1 (Table 1). Furthermore, the flexible segments of the B2\* state are the same as defined for the B1 state in the previous section, and differences of RMSf values of the individual residues for the B1 and B2\* states are also relatively small (compare Figures 2 and 3).

The average structures of the B1 and B2\* states are representative of their conformational ensemble as inferred from the corresponding RMSd vs time plots using the average structures as references (Figures S11 and S12 in Supporting Information). Computation of the  $\alpha$ -carbon distances between the average B1 and B2\* structures as a function of the residue number shows that the structural differences are relatively small and mainly refer to the helix H2, the loops C5 and C7, and the turn T5 (Figure 4).

**Table 2.** Secondary Structure Elements Description of Crystal Structure of Cyt Segments

residues	secondary structure type	label	segments <sup>a</sup>
1–4	coil (aminoterminal)	CAT	F1
5–14	helix	H1	R1
15–18	hydrogen bonded turn	T1	
19–20	coil	C1	
21–24	hydrogen bonded turn	T2	F2
25	coil	C2	
26–29	hydrogen bonded turn	T3	
30–31	coil	C3	R2
32–37	hydrogen bonded turn	T4	
38–39	sheet	E1	
40–46	hydrogen bonded turn	T5	F3
47–49	coil	C4	
50–54	helix	H2	
55–57	coil	C5	
58–59	sheet	E2	
60	coil	C6	R3
61–68	helix	H3	
69–78	hydrogen bonded turn	T6	F4
79–87	coil (omega loop)	C7	
88–102	helix	H4	R4
103–104	coil (carboxylterminal)	CCT	F5
105	heme	HEME	

<sup>a</sup> Grouped secondary structure elements classified as flexible (F) and rigid (R) segments.

Interestingly, a comparison of Figures 2 and 4 indicates that external electric fields have a stronger impact on the structure of the native protein than dissociation of the Met80 axial ligand.

As for the case of the B1 state, application of a homogeneous electric field to B2\* causes distortions of the protein structure (Figure 3). The EF-induced structural changes of state B2\* are located in the same secondary structure elements as for the B1 state, i.e., the flexible segments, although for B2\* the effect is more pronounced. The most significant changes refer to the segment F3, with the H2 helical structure being almost completely lost.

The magnitude of the electric field effect can be better appreciated by computing the  $\alpha$ -carbon distances between average structures as a function of the residue number. As shown in Figure 5, the B2EF\* structure is significantly distorted with respect to both the B2\* and the B1EF states. The structural differences between the B1EF and B2EF\* states, which correspond to the rupture of the Fe–Met80 bond in the presence of an electric field, are mainly located in the F2, F3, and F4 segments. In the latter case, the loop C7, which contains Met80, experiences the largest distortions.

A more detailed analysis shows that in the B2\* state the sulfur atom of Met80 remains at about 3 Å away from the heme iron, i.e., at a 0.7 Å longer distance than in the bound state, during the first 10 ns of the simulation, and after that, the distance fluctuates in abrupt jumps between 3.5 and 5 Å (Figure 6, upper panel). This variation is exclusively caused by free rotation of the dihedral angle CA–CB–CG–SD of the Met80 residue (Figure S13 in Supporting Information). In contrast, upon application of an electric field, the sulfur atom immediately moves away from the iron to about 6–8 Å, i.e., more than

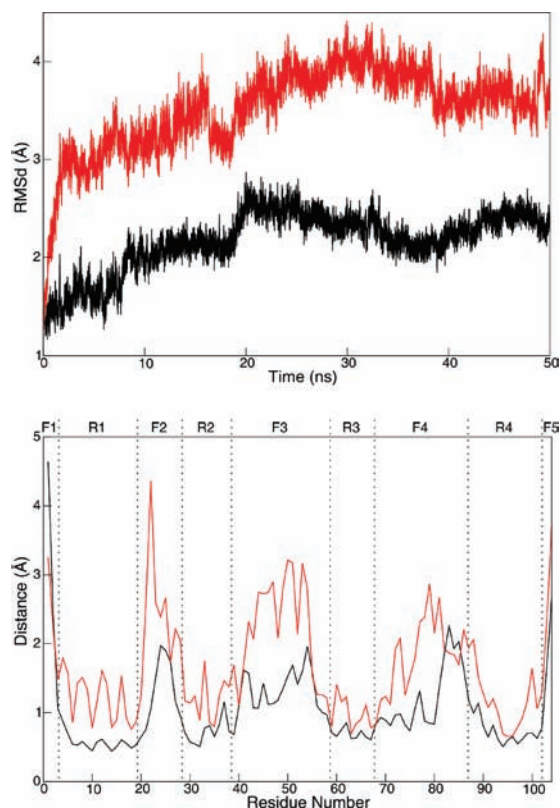


**Figure 3.** Upper panel: time evolution of RMSd for the B2\* (black) and B2EF\* (red) states with respect to the X-ray crystal structure. Lower panel: root mean square fluctuations (RMSF) versus residue number for both the B2\* (black line) and B2EF\* (red line) states.

attributable to a simple rotation of the dihedral angle, where it remains for about 20 ns. For the rest of the simulation time the distance presents large fluctuations, but on average the distances remain larger than in the absence of the electric field. The effect is presented in Figure 6 (lower panel) in terms of density populations as a function of Fe–Met80 distances for the B2\* and B2EF\* states. It is clear that the electric field pushes the unbound Met80 away from the metal center.

The results discussed above demonstrate that EF strengths of  $25 \text{ mV } \text{Å}^{-1}$  are sufficient to induce significant changes in the structure and mobility of the protein. The effect is primarily ascribed to the alignment and polarization of structural elements of the protein and can be analyzed by computing the origin-independent dipole moment modules ( $|\bar{\mu}|$ ) for the different segments and the angle cosines ( $\cos \varphi$ ) between the dipole vectors of the segments and of the whole protein (Table 3). It should be noted that in the presence of the EF the protein dipole is aligned with the EF vector, and therefore, the  $\cos \varphi$  values quantify the alignment of the segment dipoles with the EF.

The first interesting finding derived from Table 3 is that in the presence of the EF the dipole moment of Cyt, both for the B1 and B2\* states, increases by a factor of ca. 3, indicating a strong polarization. For each individual segment the effect of the EF depends on its orientation and possibilities of rotation. Rigid segments in general are not significantly polarized by the EF, although they can reorient as a result of deformations of the neighboring flexible segment. For segments such as R1 and R3, which cannot rotate and whose dipoles are oriented antiparallel to the protein dipole, the field reduces their dipole modules. In contrast, dipoles of mobile fragments should be aligned and reinforced by the EF. This is the case for most

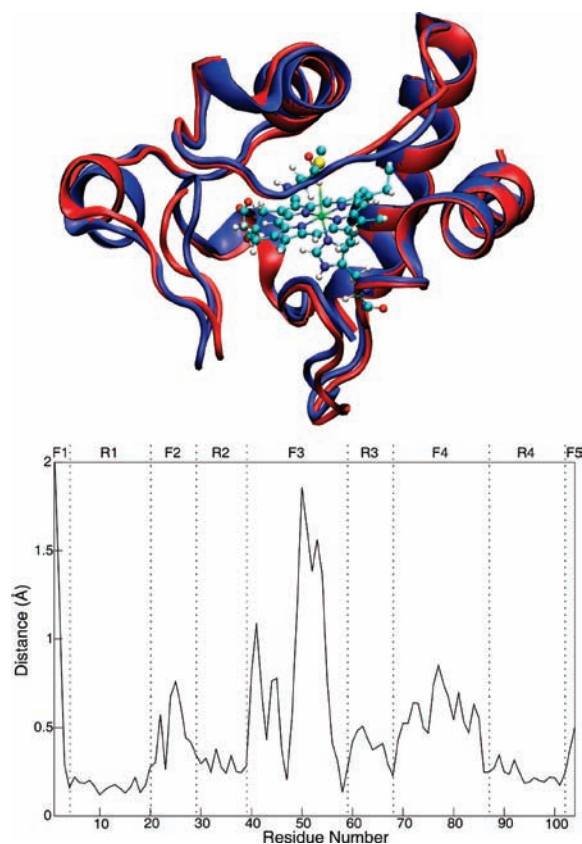


**Figure 4.** Upper panel: B1 (blue) versus B2\* (red) average structures. Lower panel: C $\alpha$ -distance versus residue plot between B1 and B2\* average structures.

flexible segments, except for the terminal coils. One of the larger effects is observed for the flexible segment F2 (see also Table S11 in Supporting Information), which in the B1 and B2\* states presents a small dipole in antiparallel orientation to the protein dipole. Upon application of the EF, both the orientation and magnitude of the F2 dipole are completely changed and aligned with the applied field.

A particularly interesting case is the behavior of the flexible segment F4, which contains the axial ligand Met80. In the B1 state, application of an EF causes a very good alignment of the segment dipole and an increase of its module by ca. 76% (see also Table S11 in Supporting Information). The effect is even more pronounced for the B2\* state, suggesting that this segment plays a crucial role in the formation and stabilization of this state in the presence of an EF. The charges of the neighboring segments also appear to be important for the formation and stabilization of the B2\* state (Table S13 in Supporting Information). The positively charged segments R4 and F4 are displaced in the direction of the EF, while the negatively charged contiguous segments R3 and F5 move in the opposite direction along with the heme group, which is also negative. The result of this movement is a slight separation of Met80 from the heme.

**3.3. Thermodynamics of the B1  $\rightarrow$  B2\* Transition.** The free energy profiles for the B1  $\rightarrow$  B2\* transition were calculated using MSM, as described in Methods, using the Fe–Met80 distance as reaction coordinate. As shown in Figure 7, the presence of the EF stabilizes the B2\* form by ca.  $5 \text{ kcal mol}^{-1}$ . Moreover, the barrier for bond breaking is reduced by ca.  $4 \text{ kcal mol}^{-1}$  (from  $11.3$  to  $7.8 \text{ kcal mol}^{-1}$ ), while the barrier for

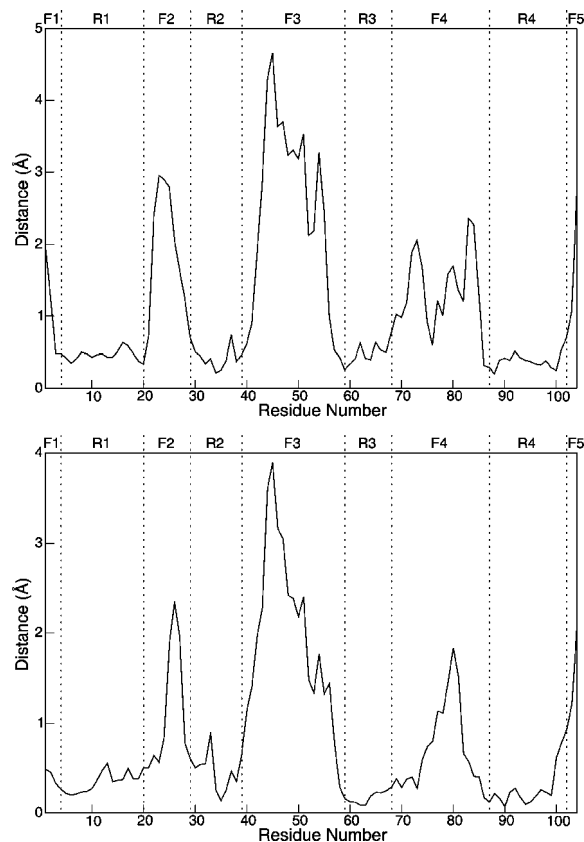


**Figure 5.** Upper panel:  $C_{\alpha}$ -distance versus residue plot between the B2\* and B2EF\* average structures. Lower panel:  $C_{\alpha}$ -distance versus residue plot between the B1EF and B2EF\* average structures.

the opposite reaction increases by 1 kcal mol<sup>-1</sup> (from 1.6 to 2.6 kcal mol<sup>-1</sup>), thereby shifting the equilibrium toward the B2\* state.

It should be noted that the minimum for the B2EF\* state appears at a Fe-Met80 distance of 6.08 Å compared to 4.67 Å for the B2\* state, in agreement with the results from Figure 6. In addition, we observe that the width of the well for the dissociated state is significantly broader in the presence of the EF, in agreement with the larger mobility predicted for B2EF\* from Figures 3 and 5.

To obtain a more detailed thermodynamic description of the reaction, we computed several parameters using the equilibrium simulations. These include the potential energy change in gas phase ( $\Delta E_{\text{gas}}$ ) and the solvation free energy change ( $\Delta G_{\text{sv}}$ ). The sum of these two terms ( $\Delta G_p = \Delta E_{\text{gas}} + \Delta G_{\text{sv}}$ ) represents an estimate of the free energy change between the corresponding states that does not include either the EF energy or the entropic contribution from the protein. Additional calculations refer to the EF energy of the protein ( $\Delta E_{\text{FE}}$ ) given by the scalar product the origin-independent dipole ( $\bar{p}$ ) and EF vectors, and the total estimated free energy change, without the entropic contribution of the protein ( $\Delta G_T = \Delta G_p + \Delta E_{\text{FE}}$ ). The results are summarized in Table 4. In gas phase the B1  $\rightarrow$  B2\* transition is energetically disfavored both in the absence and in the presence of an applied EF. This result is consistent with the loss of native interactions as a consequence of the dissociation process.

Transitions involving the passage from a state without EF to a state with EF are even more disfavored as a result of the protein deformation introduced by the EF, as it implies an important loss of internal interactions. Solvation partially

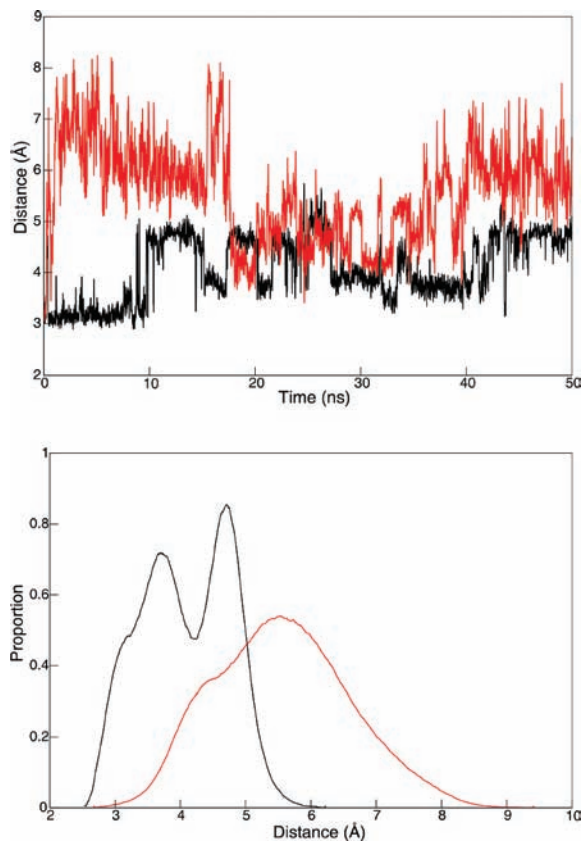


**Figure 6.** Upper panel: time evolution of Fe-Met80 distance for B2\* (black line) and B2EF\* (red line). Lower panel: density population of the Fe-Met80 distance during the time of the simulation for B2\* (black line) and B2EF\* (red line) states.

**Table 3.** Mean Dipolar Moment Module ( $|\bar{p}|$ ) of the Flexibility Segments of the Four States of Cyt in Debye and Mean Cosine of the Angle between the Total Dipole and the Dipole of the Segment ( $\cos \varphi$ )

	B1		B1EF		B2		B2EF	
	$ \bar{p} $ (D)	$\cos \varphi$	$ \bar{p} $ (D)	$\cos \varphi$	$ \bar{p} $ (D)	$\cos \varphi$	$ \bar{p} $ (D)	$\cos \varphi$
total	132.1	1	425.4	1	147.1	1	451.1	1
F1	18.1	-0.18	17.9	0.57	31.0	-0.01	21.6	0.61
R1	103.6	-0.26	85.9	-0.10	101.8	-0.24	94.4	0.12
F2	19.1	-0.53	68.0	0.92	17.9	-0.37	72.2	0.89
R2	26.4	-0.11	35.8	0.24	29.0	0.09	34.7	-0.07
F3	26.2	0.25	34.4	0.76	22.0	0.44	55.5	0.74
R3	34.2	-0.45	30.6	0.11	35.1	-0.50	27.5	-0.23
F4	44.0	0.60	77.4	0.91	37.5	0.68	91.4	0.94
R4	55.2	-0.29	53.1	0.02	56.6	-0.13	50.3	0.07
F5	18.9	0.15	19.1	0.85	19.0	0.44	19.1	0.80

compensates the energetic cost of destabilizing internal interactions, as can be inferred from the  $\Delta G_p$  values obtained for all the possible transitions. Additional stabilization is gained by the alignment of the protein dipole with the EF vector ( $\Delta E_{\text{EF}}$ ). Taking into account all these effects ( $\Delta G_T$ ), the calculations predict an energetically favored B1  $\rightarrow$  B2\* transition only when the process occurs in the presence of a moderate EF.

Free energy profiles obtained by MSMD (Figure 7) and thermodynamic parameters obtained from equilibrium computations (Table 4) cannot be directly compared. However, both types of calculations yield the same qualitative picture, which is also consistent with the results from the MD simulations, i.e., the B1  $\rightarrow$  B2\* transition is favored in the presence of an EF.

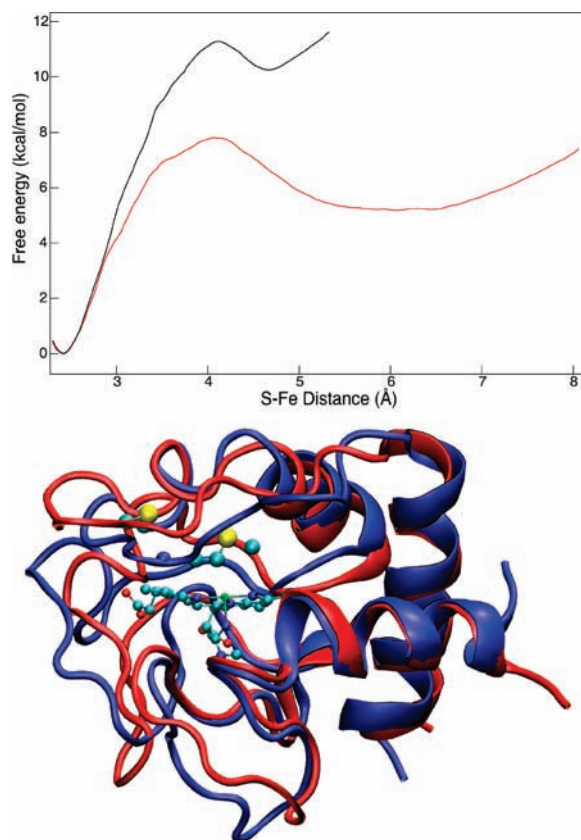


**Figure 7.** Upper panel: free energy profile obtained for the dissociation without (black) and with EF (red). Lower panel: dissociated states, B2\* (blue) and B2EF\* (red) structures.

**Table 4.** Changes in Thermodynamic Parameters for Possible Transitions in Cyt<sup>a</sup>

transition	$\Delta E_{\text{gas}}$	$\Delta G_{\text{SV}}$	$\Delta G_{\text{P}}$	$\Delta E_{\text{FE}}$	$\Delta G_{\text{T}}$	$-T\Delta S_{\text{K}}$	$-T\Delta S_{\text{S}}$
B1 → B2	66.3	-34.5	31.9	0	31.9	-46.7	-46.3
B1EF → B2EF	58.9	-57.1	1.8	-5.6	-3.8	-43.9	-43.1
B1 → B1EF	613.8	-537.7	76.1	-82.8	-6.7	-57.2	-55.1
B2 → B2EF	606.4	-560.4	46.0	-88.4	-42.4	-54.4	-51.9
B1 → B2EF	672.7	-594.9	77.9	-88.4	-10.5	-101.1	-98.2

<sup>a</sup> Thermodynamic parameters: the potential energy change of the protein in the gas phase ( $\Delta E_{\text{gas}}$ ); the solvation free energy change using a PB method ( $\Delta G_{\text{SV}}$ );  $\Delta G_{\text{P}} = \Delta E_{\text{gas}} + \Delta G_{\text{SV}}$ ; origin-independent EF energy ( $\Delta E_{\text{FE}}$ );  $\Delta G_{\text{T}} = \Delta G_{\text{P}} + \Delta E_{\text{FE}}$ ; the protein entropy change using the Karplus et al. method ( $\Delta S_{\text{K}}$ ) and using the Schlitter et al. method ( $\Delta S_{\text{S}}$ ).  $T = 300$  K. All values are in kcal/mol.

Entropy changes associated to the different possible transitions were calculated using two independent methods developed by Karplus et al.<sup>46</sup> ( $\Delta S_{\text{K}}$ ) and by Schlitter et al.<sup>45</sup> ( $\Delta S_{\text{S}}$ ), respectively. Because energy and entropy terms were computed using different methodologies, they cannot be combined. Nevertheless, the tendency is clear. All transitions represented in Table 4 imply an entropy rise as they are associated to a loss of internal interactions with the consequent increase of protein flexibility, as inferred from the dynamic studies presented in the previous sections. Note that the application of an EF produces an entropy rise even larger than that for the dissociation of Met80. Consequently, the largest entropy change is predicted for the B1 → B2EF\* transition.

In summary, it can be concluded that the application of an EF to the native Cyt (B1) favors energetically and entropically the dissociation of the Fe-Met80 bond. The energetic cost of bond breaking is compensated by the stabilizing effect of the

EF. This includes energetic stabilization through alignment of individual segments and more negative solvation energy, as well as an entropic contribution that originates in the larger flexibility of the partially unfolded protein.

## Discussion

The primary effect of applying an electric field along the  $z$  axis of modulus  $F$  to a chemically reacting system is an alteration of the energy change associated with the reaction ( $\Delta\Delta E^F$ ), which is mainly determined by the dipole moment change ( $\Delta\mu^0$ ) and the polarizability change ( $\Delta\alpha$ ) of the reaction in the direction of the electric field vector:<sup>31</sup>

$$\Delta\Delta E^F \cong -\Delta\mu_z^0 F - \frac{1}{2}\Delta\alpha_z F^2 \quad (10)$$

The polarizability change, in turn, has an electronic and a nuclear contribution. For small and rigid molecules the first component dominates. This is, for example, the case of isolated iron porphyrins that have been used as models of the redox center of Cyt.<sup>31</sup> The results from these previous studies demonstrate that the effect of an external EF on the stability of the Fe-Met bond is only marginal at biologically relevant field strengths and, therefore, cannot be the explanation for the B1 → B2 transition experimentally observed for Cyt.

On the other hand, for proteins containing charged residues and flexible side chains, nuclear polarizability may become the main source of response to an applied field. As shown in the present work, this is the case with Cyt. Application of an external EF to native (B1) Cyt produces a distortion and an increase of the mobility of the flexible segments of the protein that favor the formation of the state B2\*. The energetic cost of partial unfolding that implies the loss of intraprotein native interactions is compensated by the alignment of the dipole vectors with the applied EF as well as by the entropy rise associated with the larger protein flexibility that is observed in the presence of the EF. Our results specifically indicate that the EF-induced loss of structure of the omega loop C7, which contains the native axial ligand Met80 and is part of the flexible segment F4, is crucial for the induction of the B1 → B2\* transition. Note that the EF strength chosen for the present study, 25 mV Å<sup>-1</sup>, has the magnitude expected for a membrane interface but is ca. 1 order of magnitude smaller than the values determined at the active site for the native protein in solution.<sup>48,49</sup>

In previous experimental studies of ferric Cyt bound to negatively charged surfaces such as coated electrodes, phospholipid vesicles, or micelles,<sup>18–22,24</sup> the structure and formation kinetics of the B2 state has been studied by various techniques. These studies have revealed that the amount of state B2 in equilibrium with the native form B1 increases with the strength of the applied electric field,<sup>50</sup> in agreement with the present calculations. Moreover, the alteration of the heme ligation is accompanied by a structural perturbation of the heme pocket and distinct changes of the tertiary structure, whereas the secondary structure remains largely unchanged compared to the native form. Resonance Raman investigations showed that, depending on the specific conditions, the 5cHS form can be in equilibrium with a six-coordinated low spin (6cLS) species, for

(48) Schweitzer-Stenner, R. *J. Phys. Chem. B* **2008**, *112* (33), 10358–10366.

(49) Manas, E. S.; Vanderkooi, J. M.; Sharp, K. A. *J. Phys. Chem. B* **1999**, *103* (30), 6334–6348.

(50) Murgida, D. H.; Hildebrandt, P. *J. Phys. Chem. B* **2001**, *105* (8), 1578–1586.



which His26 (or His33) has been suggested as the sixth axial ligand on the basis of indirect evidence.<sup>51</sup> The calculations in the present work refer to a Cyt species with the Met80 ligand already removed from the heme iron but with a starting protein structure yet similar to the native state. In this sense, it may be considered as a precursor B2\* of the experimentally characterized B2 state. It is, therefore, interesting to note that the predicted EF-induced destabilization on the nanosecond time scale specifically includes the segment F2, which as inferred from the experimental data must undergo a substantial displacement during formation of the 6cLS-B2 form.<sup>22,47</sup>

The so-called alkaline transition also involves the rupture of the Fe-Met80 bond<sup>52</sup> and is favored under mild denaturing conditions,<sup>53</sup> most likely because of destabilization of the flexible loop F4. Recent NMR studies have shown that nitration of the exposed Tyr74 of Cyt, which has been identified as relevant in oxidative stress and apoptosis, promotes the B1 → B2 transition.<sup>12</sup> The results were ascribed to the destabilizing steric effect of the nitro group on the mobile C7 omega loop and is probably further destabilized in the presence of an EF. Thus, it appears that the structural lability of the C7 omega loop facilitates the detachment of the Met80 ligand under a variety of conditions, including those that are relevant in living cellular systems such as high electric fields or chemical modifications by NO. The reason why the structural lability of Cyt that leads to the formation of the state B2 has been preserved during evolution is probably related to the specific biological functions of the states B1 and B2.

The electron carrier function can only be exerted in state B1 and thus in the low EF regime beyond the level that induces the state B2. In contrast to state B2, state B1 exhibits a redox potential that allows both the reduction by complex III and the oxidation of CcO. Low EF strengths also ensure a rapid interprotein electron transfer, whereas with increasing field strengths protein reorientation of Cyt in the transient complexes with its redox partners is expected to be slowed down and thus to become rate-limiting as concluded from recent studies of Cyt in biomimetic model systems.<sup>29,54</sup> At sufficiently high EF strengths, the ferric Cyt is converted to the B2 state which, due to its negative redox potential, blocks the reduction of the heme. If this transition occurs within the Cyt/CcO complex subsequent to the interprotein electron transfer, it would prevent possible unproductive back electron transfer to Cyt. Such a mechanism has been previously suggested to support the unidirectionality of the electron flow.<sup>24,54</sup> However, the main effect of B2 formation would be that the electron transfer from complex III to CcO is interrupted.

The variation of the EF strength between values that are or are not sufficient for inducing the B2 formation may be related to changes of the transmembrane potential. Such changes might result from fluctuations of the proton gradients built up and consumed in the respiratory chain. Thus, it has been suggested that the EF-induced formation of B2 may constitute a feedback regulatory mechanism to avoid unproductive oxygen consumption.<sup>24,54</sup>

Formation of the B2 state is also associated with the gain of a quite different function, as inferred from recent studies using the M80A mutant of Cyt as a model system for the state B2<sup>26</sup> and other biomimetic systems.<sup>13,14</sup> Detachment of the axial ligand Met80 results in an increased peroxidase activity of Cyt, which is involved in oxidative sensing and signaling of apoptosis via cardiolipin oxidation and conducts to Cyt release from the mitochondria to the cytoplasm and nucleus, where activation of caspases and other yet unknown functions are promoted.<sup>26</sup>

In summary, Cyt exerts at least two qualitatively different physiological functions related to life and death of cells. In both cases crucial processes occur at the level of membrane interfaces under the influence of variable EFs, which as shown here have the potential to control Cyt structure and function.

## Conclusions

Molecular dynamics simulations show that electric fields of 25 mV Å<sup>-1</sup>, i.e., one-fourth of the upper values found at membrane interfaces, induce an increased mobility and structural distortion of key protein segments of Cyt, leading to the dissociation of the sixth axial ligand Met80 from the heme. The resulting five-coordinated high spin species is characterized by a drastically lowered reduction potential and by an increased peroxidase activity. On the basis of these results it is proposed that the variable transmembrane potential may modulate the structure of Cyt, thus constituting a switch from its redox function in the respiratory chain to peroxidase function in the early events of apoptosis.

**Acknowledgment.** This work was financed by ANPCyT (PICT07-01650, PICT06-25667, PICT2006-459), UBA (08-X625), CONICET, the Volkswagen Stiftung (I/80816), and the DFG (Unicat). P.M.D. and D.A.P. thank CONICET for their Ph.D. fellowships. F.D., D.A.E., D.H.M., and M.A.M. are members of CONICET. The Open Science Grid (OSG) supported by the National Science Foundation and the U.S. Department of Energy's Office of Science is gratefully acknowledged. Special thanks to Adrian Roitberg and Adrian Turjanski for providing equipment.

**Supporting Information Available:** RMSd plots using average structures as references for the four states. Methionine rotating dihedral angle of the B2 state. Tables with the segment dipole component changes ( $\Delta p_z$ ) and table showing the charges and dipole moments for secondary structure elements. Complete data for the thermodynamic parameters for the corresponding transitions in Cyt. This material is available free of charge via the Internet at <http://pubs.acs.org>.

JA906726N

- (51) Oellerich, S.; Lecomte, S.; Paternostre, M.; Heimburg, T.; Hildebrandt, P. *J. Phys. Chem. B* **2004**, *108* (12), 3871–3878.
- (52) Verbaro, D.; Hagarman, A.; Soffer, J.; Schweitzer-Stenner, R. *Biochemistry* **2009**, *48* (13), 2990–2996.
- (53) Maity, H.; Rumbley, J. N.; Englander, S. W. *Proteins* **2006**, *63* (2), 349–355.
- (54) Murgida, D. H.; Hildebrandt, P. *Chem. Soc. Rev.* **2008**, *37* (5), 937–945.